

E3C for Computational Homogenization in Nonlinear Mechanics

Stephan Wulfinghoff^a, Jan Hauck^a

^a*Computational Materials Science, Department of Materials Science, Kiel University, Kaiserstr. 2, 24143
Kiel, Germany
swu@tf.uni-kiel.de*

Abstract

In computational homogenization, a fast solution of the microscopic problem can be achieved by model order reduction in combination with hyper-reduction. Such a technique, which has recently been proposed in the context of magnetostatics, is applied to nonlinear mechanics in this work. The method is called 'Empirically Corrected Cluster Cubature' (E3C), as it combines clustering techniques with an empirical correction step to compute a novel type of integration points, which does *not* form a subset of the finite element integration points. The method is adopted to the challenges arising in nonlinear mechanics and is tested in plane strain for different microstructures (porous and reinforced) in dependence of the material nonlinearity. The results show that hyper-reduction errors $\lesssim 1\%$ can be achieved with a comparably small number of integration points, which is in the order of the number of modes. A two-scale example is provided and the research code can be downloaded.

Keywords: Computational homogenization, Mechanics, Model order reduction, Hyper-reduction

1 Introduction

In computational homogenization, much research has been devoted to the acceleration of the microscopic computations since the emergence of the FE²-method (Smit et al., 1998; Miehe et al., 1999; Kouznetsova et al., 2001). For brevity, we restrict ourselves here to the discussion of reduced-order models or, more specifically, Galerkin-projection methods. These exploit that the solution of the micro-problem can often be described in a lower-dimensional subspace, which is empirically accessible using, e.g., the proper-orthogonal decomposition (POD) (see Yvonnet and He, 2007, for an early two-scale method). This shifts the computational bottleneck from the solution of the global (microscopic) equation system to the evaluation of the material law(s) at the integration points of the underlying finite element mesh. Hyper-reduction methods (Ryckelynck, 2009) greatly reduce of this latter computational burden (e.g., Barrault et al., 2004; Chaturantabut and Sorensen, 2009; Carlberg et al., 2011), but often lack robustness (as discussed by van Tuijl et al., 2018; Brands et al., 2019). The empirical cubature method (ECM, Hernandez et al., 2017) is amongst the most successful methods and identifies a small subset of the finite element integration points with optimized weights. It preserves many advantageous properties (e.g., convexity) of the underlying micro-problem and is often the method of choice (e.g., Hernández, 2020; Lange et al., 2024). The Empirically Corrected Cluster Cubature (E3C) method (Wulfinghoff, 2024a), which is the method used here, is influenced by the ECM and related works (Hernández et al., 2014). It departs from the assumption that the hyper-reduced integration points have to be picked from the finite element model and instead defines generalized integration points in strain space. This idea was also used in a recent work by one of the authors (Wulfinghoff, 2024b), motivated by more traditional semi-analytical homogenization (Ponte Castañeda, 2016). Attentive readers will realize that

the mechanical theory presented as follows is in large parts almost identical to the magnetic derivation published previously, but with magnetic quantities replaced by mechanical ones.

2 Microscopic boundary value problem

The problem under consideration is a microscopic boundary value problem (BVP) with an unknown position-dependent strain

$$\boldsymbol{\varepsilon}(\mathbf{x}) = \text{sym}(\text{grad}(\mathbf{u})) = \bar{\boldsymbol{\varepsilon}} + \tilde{\boldsymbol{\varepsilon}}(\mathbf{x}) = \bar{\boldsymbol{\varepsilon}} - \text{sym}(\text{grad}(\tilde{\mathbf{u}})). \quad (1)$$

In this context, $\boldsymbol{\varepsilon}$ consists of the macroscopic¹ strain $\bar{\boldsymbol{\varepsilon}}$ and the strain fluctuation $\tilde{\boldsymbol{\varepsilon}}(\mathbf{x})$. The primary unknown is the fluctuation $\tilde{\mathbf{u}}(\mathbf{x})$ of the displacement field $\mathbf{u}(\mathbf{x})$. It is assumed that the fluctuation $\tilde{\mathbf{u}}(\mathbf{x})$ is periodic. The linear momentum balance in strong and weak form is expressed as follows:

$$\text{div}(\boldsymbol{\sigma}) = \mathbf{0}, \quad \int_{\Omega} \delta \tilde{\boldsymbol{\varepsilon}} : \boldsymbol{\sigma} \, d\Omega = 0, \quad (2)$$

In the aforementioned equation $\delta \tilde{\boldsymbol{\varepsilon}} = -\text{grad}(\delta \tilde{\mathbf{u}})$ is the variation of $\tilde{\boldsymbol{\varepsilon}}$ and Ω denotes the domain of the periodic microstructure. For the Cauchy stress we assume a position dependent material law, which accounts for microstructure heterogeneities:

$$\boldsymbol{\sigma} = \boldsymbol{\sigma}(\mathbf{x}, \boldsymbol{\varepsilon}). \quad (3)$$

3 Galerkin projection

We approximate the displacement fluctuation $\tilde{\mathbf{u}}$ in a low-dimensional subspace:

$$\tilde{\mathbf{u}}(\mathbf{x}) = \sum_{k=1}^{N_{\text{md}}} \xi_k \tilde{\mathbf{U}}_k(\mathbf{x}). \quad (4)$$

Here, $\tilde{\mathbf{U}}_k(\mathbf{x})$ are the given modes² and $\underline{\xi} = (\xi_1, \dots, \xi_{N_{\text{md}}})$ are the unknown mode coefficients. We define associated strain modes $\tilde{\boldsymbol{\varepsilon}}_k(\mathbf{x}) = \text{sym}(\text{grad}(\tilde{\mathbf{U}}_k(\mathbf{x})))$, and express the strain as follows:

$$\boldsymbol{\varepsilon}(\mathbf{x}) = \bar{\boldsymbol{\varepsilon}} + \sum_{k=1}^{N_{\text{md}}} \xi_k \tilde{\boldsymbol{\varepsilon}}_k(\mathbf{x}). \quad (5)$$

In our case, we obtain the strain modes from a finite element (FE) model with integration points \mathbf{x}^p ($p = 1, \dots, N_{\text{ip}}^{\text{FE}}$). Therefore, we obtain for the Galerkin-projected weak form (see Eq. (2)):

$$\sum_{k=1}^{N_{\text{md}}} \delta \xi_k \int_{\Omega} \tilde{\boldsymbol{\varepsilon}}_k : \boldsymbol{\sigma} \, d\Omega \approx \sum_{k=1}^{N_{\text{md}}} \delta \xi_k \underbrace{\left(\sum_{p=1}^{N_{\text{ip}}^{\text{FE}}} \tilde{\boldsymbol{\varepsilon}}_k(\mathbf{x}^p) : \boldsymbol{\sigma}(\mathbf{x}^p, \boldsymbol{\varepsilon}(\mathbf{x}^p)) \Omega_{\text{FE}}^p \right)}_{=: R_k} = \delta \underline{\xi} \cdot \underline{R} = 0. \quad (6)$$

¹At this stage, $\bar{\boldsymbol{\varepsilon}}$ is assumed given.

²The modes $\tilde{\mathbf{U}}_k(\mathbf{x})$ are assumed normalized and may be obtained from a representative set of finite-element simulations (snapshots) via proper orthogonal decomposition. This procedure is well documented in the cited literature and is not repeated here.

In this context, Ω_{FE}^p are the integration domains of the FE integration points. We define the residual vector \underline{R} , which must vanish since $\delta\underline{\xi}$ is arbitrary:

$$\underline{R} = \begin{pmatrix} R_1 \\ \vdots \\ R_{N_{\text{md}}} \end{pmatrix} = \underline{0}. \quad (7)$$

The microscopic problem is solved by identifying the unknown mode coefficients $\underline{\xi}$, which satisfy Eq. (7) for a given $\bar{\boldsymbol{\varepsilon}}$. Finally, the macroscopic stress $\bar{\boldsymbol{\sigma}}$ is computed by:

$$\bar{\boldsymbol{\sigma}} = \langle \boldsymbol{\sigma} \rangle = \frac{1}{\Omega} \int_{\Omega} \boldsymbol{\sigma} \, d\Omega \approx \frac{1}{\Omega} \sum_{p=1}^{N_{\text{ip}}^{\text{FE}}} \boldsymbol{\sigma}(\mathbf{x}^p, \boldsymbol{\varepsilon}(\mathbf{x}^p)) \Omega_{\text{FE}}^p. \quad (8)$$

4 Hyper-reduction

4.1 Hyper-reduction based on *k*-means

This hyper-reduction method aims to reduce the computational cost associated with evaluating Eqns. (6) and (8) by identifying a strongly reduced set of $N_{\text{ip}}^{\text{HR}} \ll N_{\text{ip}}^{\text{FE}}$ integration points:

$$R_k \approx \sum_{q=1}^{N_{\text{ip}}^{\text{HR}}} \tilde{\boldsymbol{\varepsilon}}_k^q : \boldsymbol{\sigma}^q \Omega^q = 0, \quad \bar{\boldsymbol{\sigma}} \approx \frac{1}{\Omega} \sum_{q=1}^{N_{\text{ip}}^{\text{HR}}} \boldsymbol{\sigma}^q \Omega^q. \quad (9)$$

Eq. (9) now sums over a significantly reduced number of integration points. The corresponding integration weights Ω^q differ from those of the FE model. The quantities Ω^q , $\tilde{\boldsymbol{\varepsilon}}_k^q$ and $\boldsymbol{\sigma}^q$ are yet to be defined.

As the main novelty of this paper, the hyper-reduction technique proposed in Wulfinghoff (2024a) is transferred to mechanics. The method is based on two ideas from literature:

- Clustering of integration points³
- Using a reduced set of integration points which preserve the original expressions in Eqns. (6) and (8) as accurately as possible for Eqns. (9)₁ and (9)₂⁴

Initially, clusters of integration points that exhibit similar strains $\boldsymbol{\varepsilon}$ are identified. This is the case for two arbitrary FE integration points with indices p_1 and p_2 if

$$\tilde{\boldsymbol{\varepsilon}}(\mathbf{x}^{p_1}) = \sum_{k=1}^{N_{\text{md}}} \xi_k \tilde{\boldsymbol{\varepsilon}}_k(\mathbf{x}^{p_1}) \approx \sum_{k=1}^{N_{\text{md}}} \xi_k \tilde{\boldsymbol{\varepsilon}}_k(\mathbf{x}^{p_2}) = \tilde{\boldsymbol{\varepsilon}}(\mathbf{x}^{p_2}). \quad (10)$$

Since this is true independent of the mode coefficients ξ_k if $\tilde{\boldsymbol{\varepsilon}}_k(\mathbf{x}^{p_1}) \approx \tilde{\boldsymbol{\varepsilon}}_k(\mathbf{x}^{p_2})$, we cluster the FE integration points in a higher-dimensional space described by

$$\tilde{\boldsymbol{\varepsilon}}(\mathbf{x}^p) = (\tilde{\boldsymbol{\varepsilon}}_1(\mathbf{x}^p), \dots, \tilde{\boldsymbol{\varepsilon}}_{N_{\text{md}}}(\mathbf{x}^p)) \in \mathbb{R}^{d \cdot N_{\text{md}}}. \quad (11)$$

For each FE integration point \mathbf{x}^p there is a counterpart $\tilde{\boldsymbol{\varepsilon}}(\mathbf{x}^p)$ in this higher-dimensional space. In case of multiple phases with constitutive laws $\boldsymbol{\sigma}^r(\boldsymbol{\varepsilon})$, clustering is performed separately for each phase $r \in (1, \dots, N_{\text{ph}})$. For the clustering we use the *k*-means algorithm (MacQueen et al.,

³For related works see, e.g., Liu et al. (2016) or Wulfinghoff et al. (2018).

⁴Compare the works on ECM in the introduction.

1967) where each FE integration point is weighted by its integration domain Ω_{FE}^p . The cluster centers \mathcal{C}^q ($q = 1, \dots, N_{\text{ip}}^{\text{HR}}$) are computed by

$$\tilde{\boldsymbol{\varepsilon}}^q = \frac{1}{\Omega^q} \sum_{p \in \mathcal{C}^q} \tilde{\boldsymbol{\varepsilon}}(\mathbf{x}^p) \Omega_{\text{FE}}^p \quad \text{with } \Omega^q = \sum_{p \in \mathcal{C}^q} \Omega_{\text{FE}}^p. \quad (12)$$

By this method we ensure that the strain $\boldsymbol{\varepsilon}^q$ at the center of a cluster \mathcal{C}^q exactly preserves the FE cluster-average (see Appendix A for a derivation):

$$\boldsymbol{\varepsilon}^q := \bar{\boldsymbol{\varepsilon}} + \sum_{k=1}^{N_{\text{md}}} \xi_k \tilde{\boldsymbol{\varepsilon}}_k^q = \frac{1}{\Omega^q} \sum_{p \in \mathcal{C}^q} \boldsymbol{\varepsilon}(\mathbf{x}^p) \Omega_{\text{FE}}^p. \quad (13)$$

Therefore, a first choice for a hyper-reduced set of $N_{\text{ip}}^{\text{HR}}$ integration points is provided in terms of the cluster centers

$$\tilde{\boldsymbol{\varepsilon}}^q = (\tilde{\boldsymbol{\varepsilon}}_1^q, \dots, \tilde{\boldsymbol{\varepsilon}}_{N_{\text{md}}}^q) \in \mathbb{R}^{d \cdot N_{\text{md}}} \quad (q = 1, \dots, N_{\text{ip}}^{\text{HR}}). \quad (14)$$

Defining the constitutive law as

$$\boldsymbol{\sigma}^q = \boldsymbol{\sigma}^q(\boldsymbol{\varepsilon}^q). \quad (15)$$

we can evaluate the hyper-reduced model in Eq. (9). Note that $\boldsymbol{\sigma}^q(\boldsymbol{\varepsilon}^q)$ depends on the phase the integration point belongs to (compare Eq. (3)) and that the reduced integration points can generally not be related to any of the original FE integration points.

4.2 Empirical correction of the k -means integration points

4.2.1 Constrained cost function minimization

In contrast to the fully integrated reduced-order model (using all $N_{\text{ip}}^{\text{FE}}$ integration points), the hyper-reduced model does not exactly satisfy the Eqns. (9)₁ and (9)₂. For the empirical correction of the hyper-reduced integration points (i.e. the cluster centers) we define a cost function e of the hyper-reduced model with respect to the fully integrated reduced-order model:

$$e(\tilde{\boldsymbol{\varepsilon}}^1, \dots, \tilde{\boldsymbol{\varepsilon}}^{N_{\text{ip}}^{\text{HR}}}) := \frac{1}{2} \sum_{s=1}^{N_{\text{full}}} \sum_{k=1}^{N_{\text{md}}} \left(\frac{1}{\Omega} \sum_{q=1}^{N_{\text{ip}}^{\text{HR}}} \tilde{\boldsymbol{\varepsilon}}_k^q : \boldsymbol{\sigma}^q(\boldsymbol{\varepsilon}^{qs}) \Omega^q \right)^2 \quad (16)$$

$$+ \frac{a}{2} \sum_{s=1}^{N_{\text{full}}} \left\| \frac{1}{\Omega} \sum_{q=1}^{N_{\text{ip}}^{\text{FE}}} \boldsymbol{\sigma}^q(\boldsymbol{\varepsilon}^{qs}) \Omega^q - \bar{\boldsymbol{\sigma}}^s \right\|^2. \quad (17)$$

Here, a is a user-defined weight (in this work $a = 1$). To obtain the quantities $\bar{\boldsymbol{\sigma}}^s$ and $\boldsymbol{\varepsilon}^{qs}$ ($s = 1, \dots, N_{\text{full}}$) we collect N_{full} simulation states with the fully integrated reduced-order model, which yield the results $\bar{\boldsymbol{\sigma}}^s$ and $\underline{\xi}^s$ and we define:

$$\boldsymbol{\varepsilon}^{qs}(\tilde{\boldsymbol{\varepsilon}}^q) = \bar{\boldsymbol{\varepsilon}}^s + \sum_{l=1}^{N_{\text{md}}} \xi_l^s \tilde{\boldsymbol{\varepsilon}}_l^q. \quad (18)$$

It is evident that the cost function (17) is similar to the works concerning the empirical cubature method (see introduction), in which it was employed to identify the reduced integration points as a subset of the FE integration points. In this case however, minimization of the cost function e indicates that we seek for those hyper-reduced integration points (i.e., the $\tilde{\boldsymbol{\varepsilon}}^q$) which

1. ensure that the hyper-reduced and fully integrated reduced-order models satisfy the reduced weak form of the linear momentum balance (Eq. (6)) for the same micro-states $\underline{\xi}$ (expressed by Eq. (16))
2. yield the same macroscopic Cauchy stress $\bar{\boldsymbol{\sigma}}$ as the fully integrated reduced-order model (incorporated by Eq. (17)).

We perform the minimization of the cost function (17) by enforcing the constraint

$$\sum_{q=1}^{N_{\text{ip}}^{\text{HR}}} \tilde{\boldsymbol{\epsilon}}^q \Omega^q = \mathbf{0} \quad (19)$$

through elimination of $\tilde{\boldsymbol{\epsilon}}^{N_{\text{ip}}^{\text{HR}}}$. By this we ensure that, at any given time, the average fluctuation vanishes:

$$\langle \tilde{\boldsymbol{\epsilon}} \rangle = \frac{1}{\Omega} \sum_{q=1}^{N_{\text{ip}}^{\text{HR}}} \sum_{k=1}^{N_{\text{md}}} \xi_k \tilde{\boldsymbol{\epsilon}}_k^q \Omega^q = \mathbf{0} \quad \Leftrightarrow \quad \langle \boldsymbol{\epsilon} \rangle = \bar{\boldsymbol{\epsilon}}. \quad (20)$$

For the minimization, we use the Fletcher-Reeves nonlinear conjugate gradient (CG) algorithm (Fletcher and Reeves, 1964) where we take the cluster centers obtained by k-means as the starting solution.

4.2.2 Training procedure

The cost function minimization described in the previous section 4.2.1 is performed using linear prescribed macroscopic strain paths $\bar{\boldsymbol{\epsilon}}(t) = \boldsymbol{\epsilon}_0 \cdot (t/T)$ with $T = 1\text{s}$ and $\boldsymbol{\epsilon}_0 = \varepsilon_0 \mathbf{N}$ ($\|\mathbf{N}\| = 1$). A plane strain situation is considered from now on using Mandel-notation:

$$\hat{\boldsymbol{\sigma}} = (\sigma_{11}, \sigma_{22}, \sqrt{2}\sigma_{12})^\top, \quad \hat{\boldsymbol{\varepsilon}} = (\varepsilon_{11}, \varepsilon_{22}, \sqrt{2}\varepsilon_{12})^\top. \quad (21)$$

The overall training procedure is divided into two stages:

1. *Unspecific training* using ~ 40 directions $\hat{\mathbf{N}}$ being equally distributed on a unit-hemisphere (due to symmetry), applying the algorithm proposed by Deserno (2004).
2. *Feedback-controlled training* based on >100 random directions $\hat{\mathbf{N}}$.

In the first stage, a fixed number of 30000 CG-iterations is applied for the cost function minimization. The second stage consists of comparing the results of the hyper-reduced and fully integrated reduced-order models and adding those five directions to the set of training directions which exhibit the largest test errors. The second stage is repeated iteratively (using 10000 CG-iterations in each iteration) until no further significant improvement is observed.

For a given simulation/direction $\hat{\mathbf{N}}$, the aforementioned test error is defined by comparing the macroscopic stress responses of the hyper-reduced (HR) with the fully integrated (FI) reduced-order model:

$$E = \frac{\max |\check{\sigma}_i^{\text{FI}} - \check{\sigma}_i^{\text{HR}}|}{\max \check{\sigma}_j^{\text{FI}} - \min \check{\sigma}_k^{\text{FI}}} \times 100\%, \quad (22)$$

where the vectors

$$\check{\boldsymbol{\sigma}}^{\text{FI}} = \begin{pmatrix} \langle \hat{\boldsymbol{\sigma}}^{\text{FI}}(t_1^*) \rangle \\ \langle \hat{\boldsymbol{\sigma}}^{\text{FI}}(t_2^*) \rangle \\ \vdots \end{pmatrix}, \quad \check{\boldsymbol{\sigma}}^{\text{HR}} = \begin{pmatrix} \langle \hat{\boldsymbol{\sigma}}^{\text{HR}}(t_1^*) \rangle \\ \langle \hat{\boldsymbol{\sigma}}^{\text{HR}}(t_2^*) \rangle \\ \vdots \end{pmatrix} \quad (23)$$

contain all macroscopic stress values at user-defined times t_1^*, t_2^*, \dots . The numerator in Eq. (22) thus represents the largest stress component deviation between the two reduced-order models amongst all considered time steps of one of the >100 random directions $\hat{\mathbf{N}}$ mentioned above.

5 Results

5.1 Porous microstructure

5.1.1 Simulation set-up

A porous microstructure with periodic boundary conditions is considered, as depicted in Fig. 1 (right). The material model applied to the matrix is the pseudo-elastoplastic Ramberg-Osgood (RO) law (Ramberg and Osgood, 1943), which is given in detail in Appendix B. The visualization in Fig. 1 (left) shows different degrees of nonlinearity in terms of the exponent p of the Ramberg-Osgood law, where the depicted values $p \in \{5, 10, 20\}$ have been chosen to be in a typical range for most metals. The mesh, consisting of bilinear quadrilaterals with single

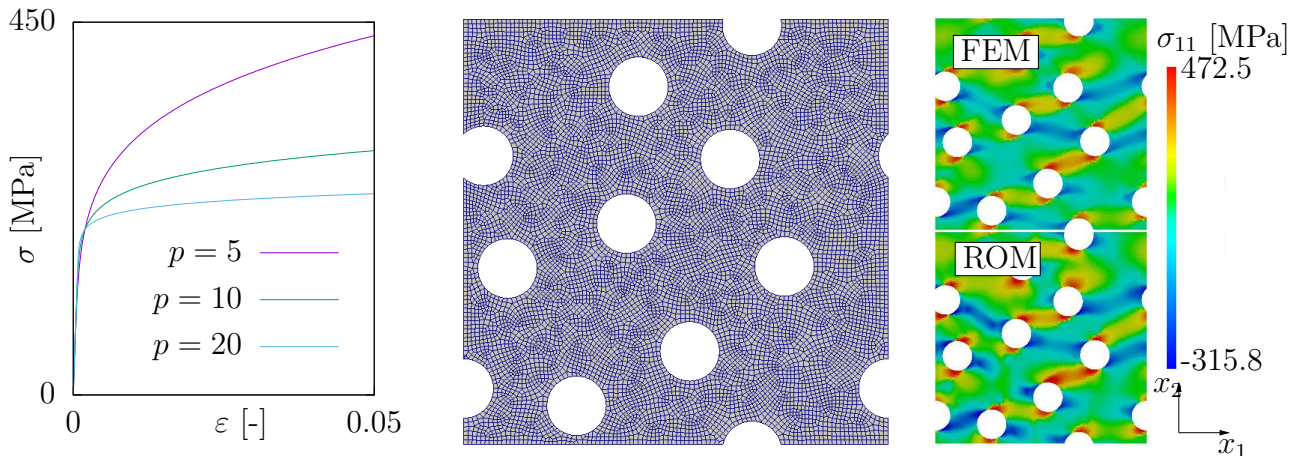


Figure 1: Left: Ramberg-Osgood law. Center: Mesh. Right: Exemplary stress comparison (ROM reconstructed with 15 IPs) at $\hat{\varepsilon} = 0.00707(1, -1, -\sqrt{2})^T$ for $p = 5$. The strain fields are not shown since they are hardly differentiable.

point integration and hourglass stabilization, is shown in Fig. 1 (center). For a comparably low exponent of $p = 5$, the fully integrated reduced-order model requires $N_{\text{md}} = 15$ modes in order to yield macroscopic stress predictions, which are reasonably close (deviations in the order of 1%) to the finite element model⁵. Keeping in mind that the material nonlinearity is moderate, this rather high number of modes illustrates that the example of a porous microstructure is challenging, which can in part be explained by intense strain fluctuations going along with the infinite phase contrast between matrix and pores.

5.1.2 Accuracy assessment

The accuracy of the hyper-reduced model is evaluated by comparing its results with its fully integrated counterpart for another set of yet another 100 simulations with random strain directions \hat{N} , which have not been considered during training (unseen data). The corresponding average and maximum errors are depicted in Fig. 2 (left) as a function of the number of integration points $N_{\text{ip}}^{\text{HR}}$. For seven integration points, the average error of 2.1% is already comparably low while the maximum error is still 7.5%. For 10 and 15 integration points, the observed errors reach the order of 1% and below. The maximum error amongst the 100 validation simulations is 1.18% for 15 integration points. The corresponding results are depicted in Fig. 2 (b). The maximum error occurs in the $\langle \sigma_{11} \rangle$ -component, as illustrated in part (c) of the same figure, showing an enlargement of the region marked by the dashed rectangle in (b). The interested reader is invited to download the code ([A preliminary set of files is provided to the reviewers here: https://cloud.rz.uni-kiel.de/index.php/s/qCMTP5ZoxHZAbCf](https://cloud.rz.uni-kiel.de/index.php/s/qCMTP5ZoxHZAbCf)).

⁵The finite element software FEAP 8.4 (Taylor, 2018) was used.

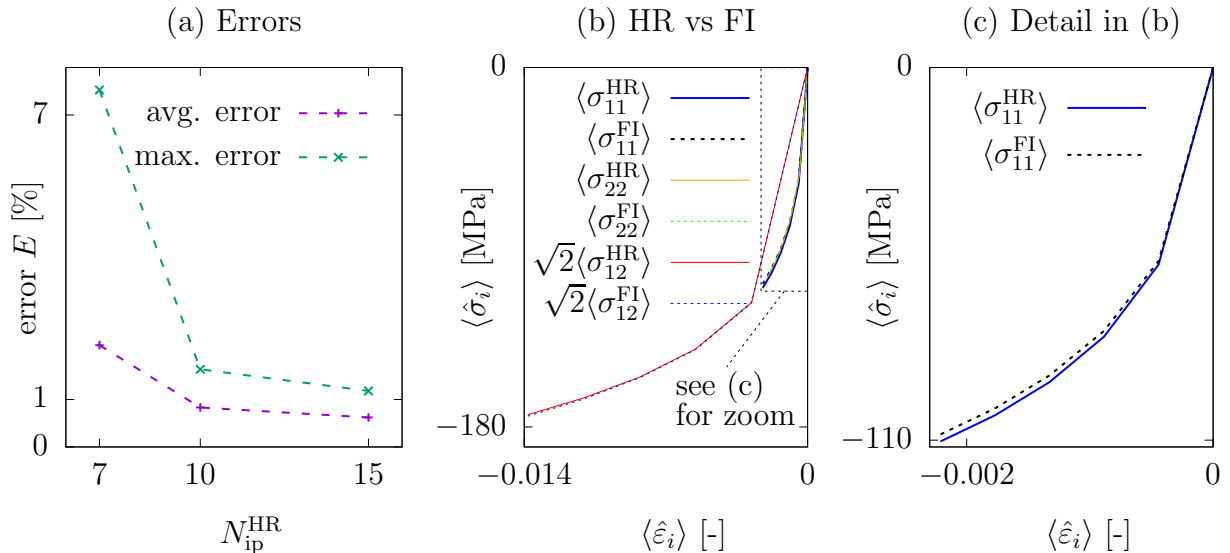


Figure 2: (a) Hyper-reduction error E (see Eq. (22)) over number of integration points N_{ip}^{HR} for $p = 5$. (b) Exemplary comparison of ROM with 15 IPs (HR) vs. full integration (FI) with the purpose to illustrate the maximum hyper-reduction error of 1.18% amongst all 100 validation simulations. (c) Enlargement of the marked region in (b), showing the $\langle \sigma_{11} \rangle$ -component.

5.1.3 Assessment of the computational effort

The probably most important quantities to assess the computational effort of the reduced-order model are the number of modes and number of integration points needed to reach a certain accuracy. The CPU-time of the hyper-reduced model with 15 integration points is on average approximately 1.1-1.3 ms per time step (on laptop hardware⁶), while it is in the order of 1.5 s for the FEM-model, yielding a speed-up roughly in the order of 1200. This figure does not include the fact that, in order to reach convergence, the hyper-reduced model often needs time steps roughly half as large as the fully integrated and finite element models.

The training effort for the different number of integration points is summarized in Tab. 1.

| N_{ip}^{HR} | 7 | 10 | 15 |
|---------------|------------|-----------|-------------|
| time | 4 min 51 s | 9 min 1 s | 18 min 24 s |

Table 1: Training effort in dependence of the number of integration points N_{ip}^{HR} for $p = 5$ and 15 modes (code not parallelized).

The depicted figures do not include the computational effort resulting from the simulations with the fully integrated reduced-order model necessary for the training. This additional effort is in the order of 8-9 minutes for the present example.

5.1.4 Influence of the nonlinearity

If the exponent p in Eq. (B.1) is increased from 5 to 10, the hardening is decreased, as illustrated in Fig. 1 (left), leading to a stronger localization of the deformation within bands connecting the pores. This observation goes hand in hand with an increased number of modes of $N_{md} = 25$ being required to capture a reasonable accuracy in terms of macroscopic stress deviations in the order of 1% between the finite element model and the fully integrated reduced-order model. This relatively high number of modes indicates the complexity of the combination of a porous microstructure with an increased nonlinearity ($p = 10$). Consistently, also an increased

⁶The CPU was an Intel CoreTM i7-8850H CPU @ 2.60GHz with 32 GB RAM.

number of $N_{\text{ip}}^{\text{HR}} = 20$ integration points is required to reach an average hyper-reduction error of $E = 1.98\%$ (see Eq. (22)), while the maximum error is 4.07%. For 30 and 40 integration points, the average error drops to 1.26% and 1.0%, respectively, while the maximum errors are given by 1.87% and 1.59%. It is noted that these error values depend on the training parameters. These have not been systematically optimized in this work, and more advanced training procedures may lead to lower errors.

5.2 Reinforced composites

5.3 Fibre-reinforced composite

5.3.1 Micro-model

Next, a fibre-reinforced composite material is investigated, the mesh of which is illustrated in Fig. 3 (left). The composite consists of elastic fibres with Young's modulus $E_{\text{F}} = 300\text{MPa}$ and Poisson's ratio $\nu_{\text{F}} = 0.25$ embedded in the Ramberg-Osgood matrix material described above with $p \in \{5, 10, 20\}$. In the nonlinear regime, the composite response to a given macroscopic stress is usually predominantly deviatoric in the sense that the spherical (volumetric) part of the macroscopic strain remains small. For that reason, the macroscopic strain directions used during the training procedure (see Sect. 4.2.2) are chosen close to the deviatoric plane, such that the macroscopic stress components remain within a reasonable range $\lesssim 400\text{MPa}$.

Depending on the value of the exponent p , 11-14 modes turn out to be sufficient to decrease the error of the fully integrated reduced order model to a negligible value in comparison with the finite element model. Figure 3 (right) summarizes the hyper-reduction error E for 100 validation simulations for exponents $p \in \{5, 10, 20\}$. Even in the most nonlinear case $p = 20$, less than 10 integration points are sufficient to reach errors $\lesssim 1\%$. In all cases, the training effort⁷ was 5-10 minutes.

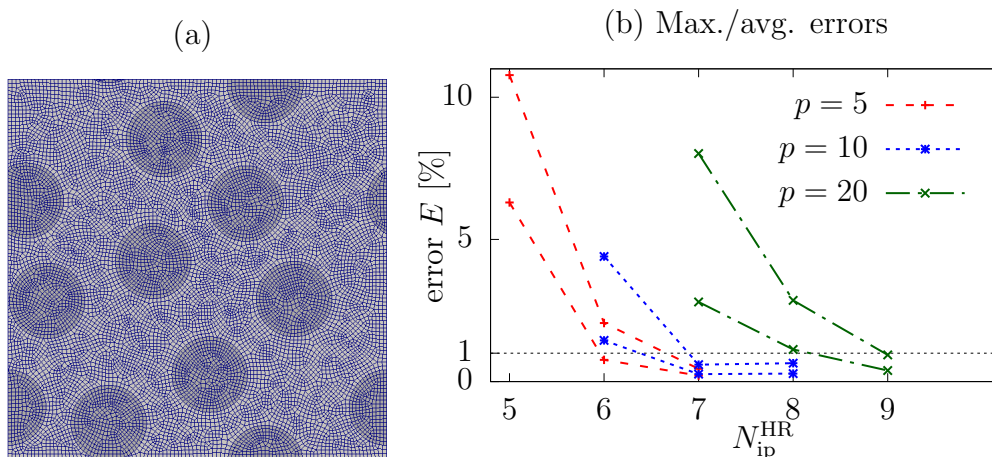


Figure 3: (a) Mesh of the reinforced composite. (b) Maximum and average hyper-reduction errors E (see Eq. (22)) over total number of integration points $N_{\text{ip}}^{\text{HR}}$. The linear-elastic fibres are represented by a single integration point.

5.3.2 Two-scale simulation

Figure 4 (left) shows an exemplary two-scale simulation of a beam, being loaded on its right end by a prescribed macroscopic displacement \bar{u}_2 in the vertical direction. The corresponding reaction force is depicted in the right part of the figure. For $p = 10$, $N_{\text{ip}}^{\text{HR}} = 8$ and a macroscopic mesh consisting of $40 \times 20 = 800$ elements, the total simulation time was $\sim 8.6\text{s}$ using 10 equal

⁷Again, this excludes the generation of the FEM-data and the simulations using the fully integrated model.

time steps. For comparison, a single scale simulation using the Ramberg-Osgood model with $p = 10$ is approximately 11 times faster, as it takes ~ 0.8 s. For a mesh with $160 \times 80 = 12800$ elements, these figures increase to ~ 146 s and ~ 20 s, respectively. In this case, the single-scale simulation is only 7.3 faster than the two-scale model. A possible explanation for the different factors is that for gradual mesh refinement, the time required to solve the global linear equation systems grows disproportionately with respect to the numbers of degrees of freedom, in contrast to the effort due to the material law evaluation. Based on this hypothesis, the aforementioned factors could further be decreased by parallelization of the assembly process, which is beyond the scope of this work.

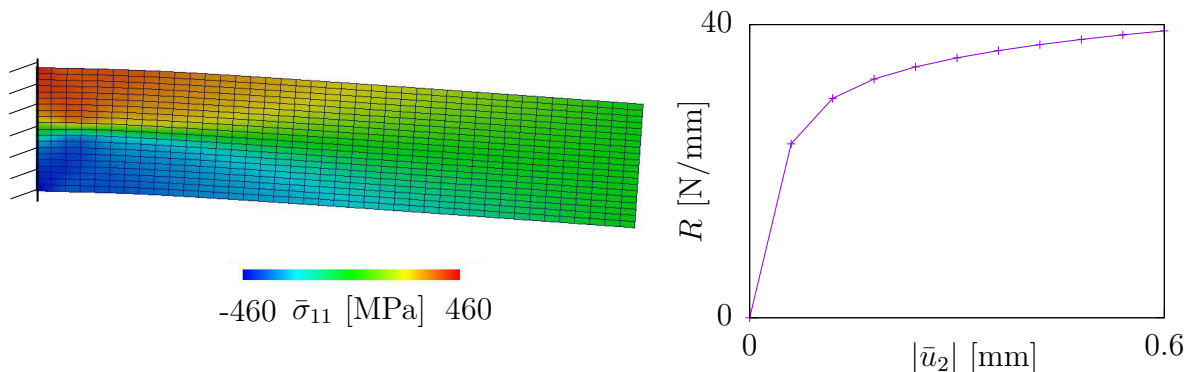


Figure 4: Left: Plane-strain two-scale simulation of a beam with dimensions 10×2 mm, being clamped on the left end. Right: Reaction force over displacement at the right end.

5.4 Composite with large fibre diameter

Next, the fibre diameter is increased (see Fig. 5, left), provoking intense strain fluctuations in between the fibres. The fully integrated reduced-order model is capable to accurately predict the finite element results with 11-14 modes, with errors typically in the order of 1% and below. For $p = 5$, the dependence of the hyper-reduction error on the number of integration points is comparable to the case with smaller fibre diameter (see red lines in Fig. 5, right). However, for $p = 20$, in total 30 integration points are required to reach errors of $\sim 1\%$ and below (green lines).

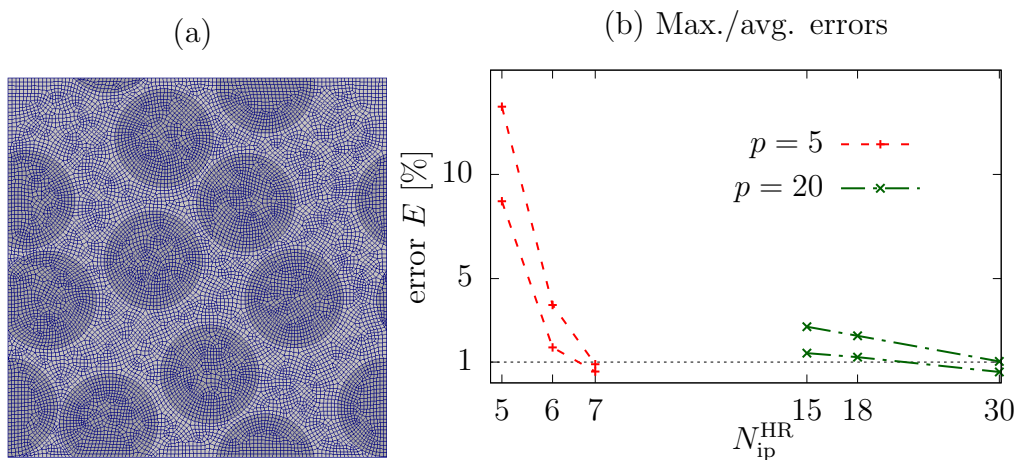


Figure 5: (a) Mesh of the reinforced composite. (b) Maximum and average hyper-reduction errors E (see Eq. (22)) over total number of integration points N_{ip}^{HR} . The linear-elastic fibres are represented by a single integration point in all cases except $p = 20$ and $N_{ip}^{HR} = 30$, where three integration points were used.

6 Summary and conclusion

The hyper-reduction technique 'Empirically Corrected Cluster Cubature (E3C)', which was recently proposed in the context of magnetostatics, has been adopted to nonlinear mechanical computational homogenization. The number of integration points needed to reach hyper-integration errors in the order of 1% depends on the microstructure and material nonlinearity, but has been found to be roughly similar to the number of modes. As the number of integration points approaches the theoretical limit⁸, it seems reasonable to focus next on reducing the number of modes (rather than integration points) to further improve performance. One approach to achieve this is problem-adopted training (Lange et al., 2024). However, the origin of the high number of modes required in certain cases (low hardening, strong fluctuations) still needs to be better understood.

Acknowledgements

This work was supported by the German Research Foundation (Deutsche Forschungsgemeinschaft, DFG) through the project A10 of the Collaborative Research Center SFB 1261 under Grant 286471992. This support is gratefully acknowledged.

Appendix A Preservation of the cluster average

The proof of Eq. (13) reads

$$\boldsymbol{\varepsilon}^q = \bar{\boldsymbol{\varepsilon}} + \sum_{k=1}^{N_{\text{md}}} \xi_k \tilde{\boldsymbol{\varepsilon}}_k^q \stackrel{(12)}{=} \bar{\boldsymbol{\varepsilon}} + \frac{1}{\Omega^q} \sum_{p \in \mathcal{C}^q} \sum_{k=1}^{N_{\text{md}}} \xi_k \tilde{\boldsymbol{\varepsilon}}_k(\mathbf{x}^p) \Omega_{\text{FE}}^p = \frac{1}{\Omega^q} \sum_{p \in \mathcal{C}^q} \boldsymbol{\varepsilon}(\mathbf{x}^p) \Omega_{\text{FE}}^p. \quad (\text{A.1})$$

Appendix B Ramberg-Osgood law

The Ramberg-Osgood law reads

$$\boldsymbol{\varepsilon} = \frac{1}{9\kappa} \text{tr}(\boldsymbol{\sigma}) \mathbf{I} + \frac{\boldsymbol{\sigma}'}{2\mu} + \frac{3}{2} \varepsilon_0 \left(\frac{\sigma_{\text{eq}}}{\sigma_0} \right)^p \frac{\boldsymbol{\sigma}'}{\sigma_{\text{eq}}} \quad (\text{B.1})$$

with the stress deviator $\boldsymbol{\sigma}'$, von-Mises stress $\sigma_{\text{eq}} = \sqrt{3/2} \|\boldsymbol{\sigma}'\|$ and material parameters in Tab. B.2 (κ and μ denote the bulk and shear modulus, respectively).

| E_{M} [GPa] | ν_{M} | σ_0 [MPa] | ε_0 [-] | p |
|----------------------|------------------|------------------|---------------------|----------|
| 210 | 0.3 | 200 | 0.001 | see text |

Table B.2: Parameters of Ramberg-Osgood matrix ('M').

References

Barrault, M., Maday, Y., Nguyen, N. C., Patera, A. T., 2004. An 'empirical interpolation method: application to efficient reduced-basis discretization of partial differential equations. *Comptes Rendus Mathématique* 339 (9), 667–672.

⁸If the number of integration points falls below the limit of $N_{\text{md}}/n_{\text{T}}$, the underlying equation systems in $\underline{\xi}$ become singular (with n_{T} being the dimension of $\hat{\boldsymbol{\sigma}}$ and $\hat{\boldsymbol{\varepsilon}}$).

- Brands, B., Davydov, D., Mergheim, J., Steinmann, P., 2019. Reduced-order modelling and homogenisation in magneto-mechanics: A numerical comparison of established hyper-reduction methods. *Mathematical and Computational Applications* 24 (1), 20.
- Carlberg, K., Bou-Mosleh, C., Farhat, C., 2011. Efficient non-linear model reduction via a least-squares Petrov–Galerkin projection and compressive tensor approximations. *International Journal for numerical methods in engineering* 86 (2), 155–181.
- Chaturantabut, S., Sorensen, D. C., 2009. Discrete empirical interpolation for nonlinear model reduction. In: *Decision and Control, 2009 held jointly with the 2009 28th Chinese Control Conference. CDC/CCC 2009. Proceedings of the 48th IEEE Conference on.* IEEE, pp. 4316–4321.
- Deserno, M., 2004. How to generate equidistributed points on the surface of a sphere. In *Polymerforschung* (Ed.).
- Fletcher, R., Reeves, C. M., 1964. Function minimization by conjugate gradients. *The computer journal* 7 (2), 149–154.
- Hernández, J., 2020. A multiscale method for periodic structures using domain decomposition and ECM-hyperreduction. *Computer Methods in Applied Mechanics and Engineering* 368, 113192.
- Hernández, J., Oliver, J., Huespe, A. E., Caicedo, M., Cante, J., 2014. High-performance model reduction techniques in computational multiscale homogenization. *Computer Methods in Applied Mechanics and Engineering* 276, 149–189.
- Hernandez, J. A., Caicedo, M. A., Ferrer, A., 2017. Dimensional hyper-reduction of nonlinear finite element models via empirical cubature. *Computer methods in applied mechanics and engineering* 313, 687–722.
- Kouznetsova, V., Brekelmans, W., Baaijens, F., 2001. An approach to micro-macro modeling of heterogeneous materials. *Computational Mechanics* 27 (1), 37–48.
- Lange, N., Hütter, G., Kiefer, B., 2024. A monolithic hyper rom fe2 method with clustered training at finite deformations. *Computer Methods in Applied Mechanics and Engineering* 418, 116522.
- Liu, Z., Bessa, M., Liu, W. K., 2016. Self-consistent clustering analysis: an efficient multi-scale scheme for inelastic heterogeneous materials. *Computer Methods in Applied Mechanics and Engineering* 306, 319–341.
- MacQueen, J., et al., 1967. Some methods for classification and analysis of multivariate observations. In: *Proceedings of the fifth Berkeley symposium on mathematical statistics and probability.* Vol. 1. Oakland, CA, USA., pp. 281–297.
- Miehe, C., Schröder, J., Schotte, J., 1999. Computational homogenization analysis in finite plasticity simulation of texture development in polycrystalline materials. *Computer methods in applied mechanics and engineering* 171 (3-4), 387–418.
- Ponte Castañeda, P., 2016. Stationary variational estimates for the effective response and field fluctuations in nonlinear composites. *Journal of the Mechanics and Physics of Solids* 96, 660–682.

- Ramberg, W., Osgood, W. R., 1943. Description of stress-strain curves by three parameters. Tech. Rep. 902, NACA.
- Ryckelynck, D., 2009. Hyper-reduction of mechanical models involving internal variables. *International Journal for Numerical Methods in Engineering* 77 (1), 75–89.
- Smit, R., Brekelmans, W., Meijer, H., 1998. Prediction of the mechanical behavior of nonlinear heterogeneous systems by multi-level finite element modeling. *Computer Methods in Applied Mechanics and Engineering* 155 (1-2), 181–192.
- Taylor, R. L., 2018. FEAP – A finite element analysis program.
- van Tuijl, R. A., Remmers, J. J., Geers, M. G., 2018. Integration efficiency for model reduction in micro-mechanical analyses. *Computational mechanics* 62, 151–169.
- Wulfinghoff, S., 2024a. Empirically corrected cluster cubature (e3c). Preprint.
URL <http://dx.doi.org/10.2139/ssrn.5043816>
- Wulfinghoff, S., 2024b. Statistically compatible hyper-reduction for computational homogenization. *Computer Methods in Applied Mechanics and Engineering* 420, 116744.
- Wulfinghoff, S., Cavaliere, F., Reese, S., 2018. Model order reduction of nonlinear homogenization problems using a hashin–shtrikman type finite element method. *Computer Methods in Applied Mechanics and Engineering* 330, 149–179.
- Yvonnet, J., He, Q.-C., 2007. The reduced model multiscale method (R3M) for the non-linear homogenization of hyperelastic media at finite strains. *Journal of Computational Physics* 223 (1), 341–368.